

Nanomanufacturing of Graphene Nanosheets through Hole Engineering

Yanan Chen^{1, (a)}, Yilin Wang^{1, (a)}, Shuze Zhu², Kun Fu¹, Xiaogang Han¹, Yanbin Wang¹, Bin Zhao¹, Tian Li¹, Boyang Liu¹, Yiju Li¹, Jiaqi Dai¹, Teng Li², John W. Connell³, Yi Lin^{4, *}, Liangbing Hu^{1, *}

¹Department of Materials Science and Engineering, University of Maryland College Park, College Park, Maryland, 20742

²Department of Mechanical Engineering, University of Maryland College Park, College Park, Maryland, 20742

³Advanced Materials and Processing Branch, NASA Langley Research Center, Hampton, VA 23681-2199

⁴National Institute of Aerospace, 100 Exploration Way, Hampton, Virginia 23666-6147

(a) Contributed equally to this work.

Email: binghu@umd.edu; yi.lin-1@nasa.gov

Key words: Graphene, Defect engineering, Moldability, High conductivity, Nanomanufacturing

Abstract

Facile and scalable fabrication of highly dense and high quality graphene films and articles is extremely attractive for a range of electronic and mechanical applications. Pristine, high quality graphene with its inherent impermeability poses challenges in fabricating dense films and thick parts with high electrical conductivity due to the difficulty in removing trapped air and/or solvents used in various fabrication methods. To overcome this deficiency, nano-holes were intentionally created in pristine graphene (“holey graphene”) with an average diameter of approximately 15 nm. The holes serve as pathways for the rapid removal of gases or liquids and enable the fabrication of dense holey graphene nanostructures. Subsequently, a high temperature process is applied to effectively repair the nano-holes and recover the high quality graphene conjugated network. Through the creation and repair of the nano-holes, dense graphene articles were created that exhibited an ultrahigh conductivity of 2209 S/cm and a high carrier mobility of $673 \text{ cm}^2\text{V}^{-1}\text{s}^{-1}$. This unique processing methodology enables the facile and scalable fabrication of high quality graphene constructs for a variety of applications.

Introduction

Graphene is a promising 2D material with excellent electrical conductivity^[1], thermal conductivity^[2], chemical and temperature resistance^[3-6], mechanical strength and low density^[7], and is ubiquitously applied in fields such as energy^[8-14], environment^[15,16], automobile and aerospace^[17]. However, the performance of graphene-based macrostructures (fibers, films, complex shapes and articles), in terms of electrical conductivity and carrier mobility^[18,19], is far less than that of an individually isolated high quality graphene sheet. This is because the effects from the limit on sheet lateral sizes, and the presence of defects become more significant as the macrostructures increase in size. Also, the current approaches to fabricate graphene-based articles often introduce defects, but those defects are difficult to fully remove, and can diminish mechanical, electrical and thermal properties. Current manufacturing methods for graphene or reduced graphene oxide (RGO) have a major limitation: difficulty in removing solvents or gases to achieve a dense structure, due to the impermeability of macroscopic stacks of such sheet-like 2D nanostructures. It has been reported that gases such as H₂ and He cannot permeate graphene nanosheets^[20] and most solvents cannot permeate intact graphene, which limits its effective manufacturing^[20]. The electrical performance of graphene film fabricated from solution exfoliated small graphene flakes is poor, with a low DC conductivity on the order of 100 S/cm^[21]. Another strategy for graphene manufacturing is to synthesize graphene oxide (GO) which allows for easier processing, followed by film fabrication, and then reduction^[22-26]. A much higher conductivity has been demonstrated by the chemical reduction or thermal reduction of GO^[27-35]. For example, the highest DC conductivity reported in chemically reduced graphene approaches 1000 S/cm^[36]. Lian et al. recently reported that a high conductivity of 1790 S/cm was achieved for pure chemically converted graphene after thermal annealing at high temperatures up to 3123K^[37]. The solution processes discussed above to process the chemically converted graphene, typically via vacuum

filtration, is time-consuming and has limitations with respect to film thickness. In addition, to achieve high electrical conductivity, the high temperature annealing process requires expensive and complicated equipment, and is time-consuming. Thus, developing a new methodology to scale-up and rapidly manufacture highly dense graphene architectures with excellent performance would be a major breakthrough.

Creating holes in the 2D material is an attractive approach as it is simple and scalable, and it solves the fundamental challenges in the ability to remove solvent and gas during article fabrication. The nano-holes enable the fabrication of dense nanostructures while also creating reactive edge sites for subsequent functionalization^[38–41]. Recently there has been much progress on the development and applications of holey graphene (h-Graphene) in energy storage (batteries, supercapacitors)^[42–45], water desalination^[46], chemical and biosensing^[47]. However, for applications requiring high electrical conductivity, the presence of holes in the final article are fundamentally problematic as they disrupt the graphitic conjugated network structure and deteriorate the original performance of high quality graphene.

In this study, a facile, scalable process is demonstrated involving the creation of nano-holes on graphene nanosheets followed by rapid thermal healing to fabricate highly dense and defect-free 2D graphene films (via vacuum filtration) and 3D graphene assemblies (via dry compression molding), as illustrated in Figure 1. Nano-holes in graphene nanosheets can be created by simply oxidizing the commercial graphene powder in hot air to selectively oxidize defective sites. The nano-holes allow for fast solvent escape when employing solution-processed methods such as vacuum filtration. In addition, the as-obtained h-Graphene powders can be pressed or molded into

an article under completely solvent-free conditions using a standard hydraulic press. After the solution-processed or dry-compression fabrication, holes on graphene nanosheets within the film or article can be rapidly closed or repaired by electrically induced thermal annealing, also known as “Joule heating”, at high temperature (~ 2700 K). Molecular dynamics (MD) modeling indicates that the holes closing or repairing mechanism involves the reconstruction of the conjugated carbon structure with carbon radicals filling up the holes under high temperature. The healed graphene architecture with closed holes exhibits excellent electrical conductivity (2209 S/cm), high electron mobility ($673 \text{ cm}^2\text{V}^{-1}\text{s}^{-1}$) and superior mechanical strength.

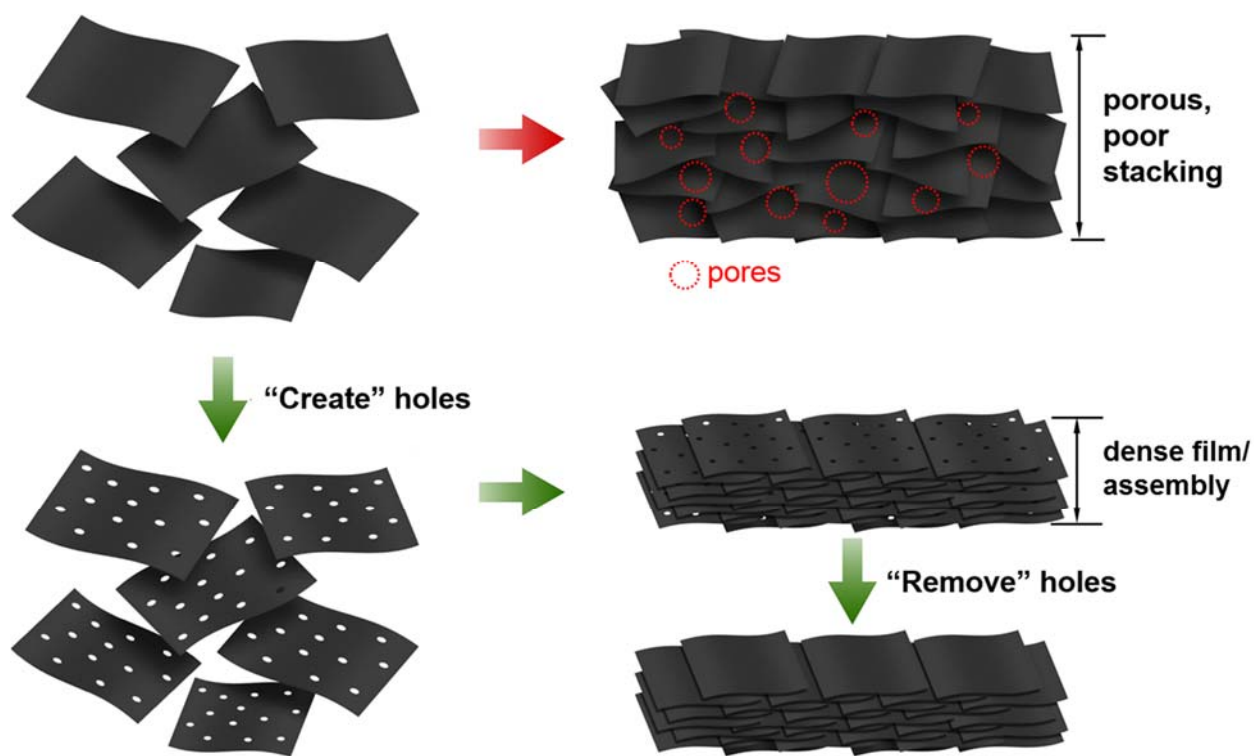


Figure 1 Schematic illustration of the process of opening and closing holes on graphene nanosheets to fabricate the highly dense and defect-free 2D graphene films and 3D graphene assemblies.

The most common methods to create defects on graphene rely on the use of chemical methods such as chemical etching with KOH and/or HNO₃, and catalytic oxidation with metal or metal oxide catalysts^[43]. In this study, no conventional chemical methods were used for the hole creation or repair^[38,42]. The simple one-step process to create holes in graphene is illustrated in Figure 2a. In a typical reaction, ~1.5 g of commercial graphene powder was placed in a quartz boat and heated in an open-ended tube furnace at ~710 K with a heating rate of 10 K/min. After 10 h, ~1.1-1.2 g h-Graphene powder was obtained. The scalability of h-Graphene produced in this reaction is only limited by the size of the heating equipment. Mechanistically, the noncrystalline and defective sites on the pristine graphene nanosheets preferentially react with oxygen under hot air, leaving nano-holes. Raman spectral profiles of the pristine graphene and h-Graphene (Figure 2b) display similar intensity ratio (~ 0.8) of D band (~ 1,350 cm⁻¹, defective carbon) to G band (~ 1,580 cm⁻¹, graphitic carbon). This suggests that almost the same amount of disordered carbon atoms are distributed on graphene nanosheets despite the new presence of the nanosized holes. This result is consistent with the above mentioned mechanistic assumption of preferential defect carbon removal. X-ray diffraction (XRD) was employed to investigate the microstructure of the starting graphene and h-Graphene (Figure 2c). Compared to that of the pristine graphene, the characteristic graphitic peak (26°) of h-Graphene was much broader, indicating more disrupted stacking of graphitic crystalline regions. The morphology of the pristine graphene nanosheets is illustrated in Figure S1~S2, showing no holes on the graphene nanosheets before treatment (Supplementary Information). Figure 2d shows a typical scanning electron microscopy (SEM) image of a h-Graphene nanosheet, indicating a large quantity of holes uniformly distributed on the nanosheet surface. These nano-holes are estimated to have an average diameter of 15 nm based on analysis

of a large number of SEM and transmission electron microscopy (TEM) images acquired at different locations of the h-Graphene specimen (Figure 2d-f).

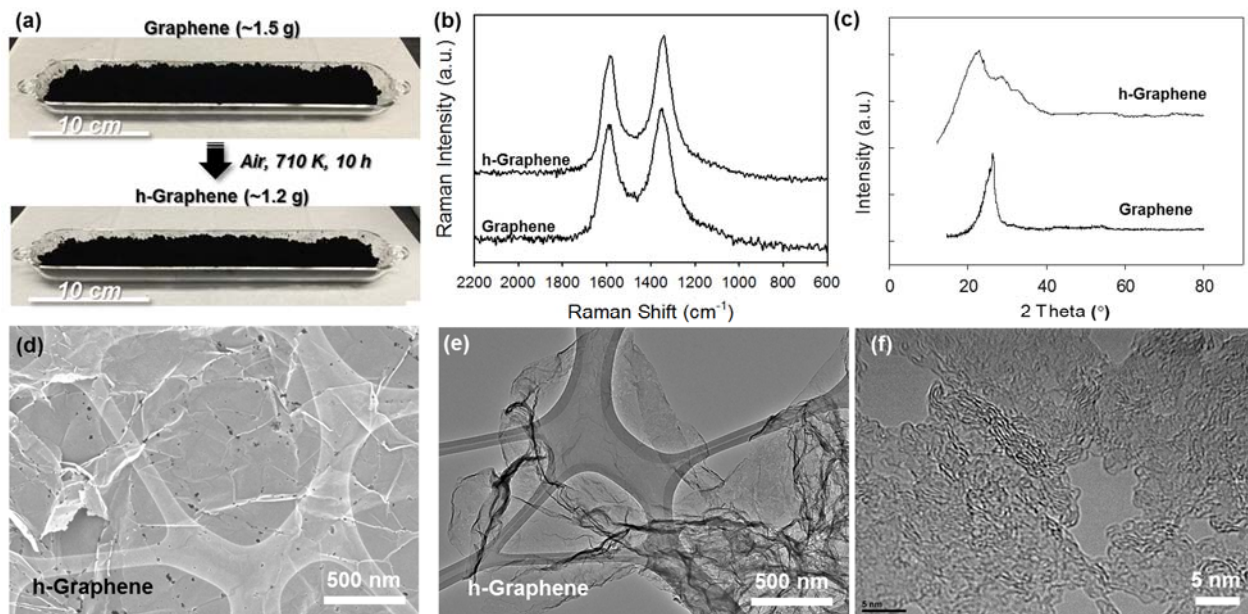


Figure 2 (a) One-step synthesis process of the h-Graphene nanosheets from commercial graphene nanosheets by heating at 710 K for 10h in air. Shown in the photographs are the same sample before (top) and after (bottom) thermal treatment. (b) Raman spectra and (c) XRD patterns of pristine graphene and h-Graphene. (d) Typical SEM and (e) TEM image of h-Graphene nanosheets. (f) High resolution TEM image of h-Graphene nanosheets. All images clearly show the nano-holes on the h-Graphene nanosheets.

The high temperature (HT) thermal behavior of h-Graphene films and assemblies were investigated next. The free-standing h-Graphene film (~5 μm in thickness) with high flexibility (Figure 3a) was fabricated by vacuum filtration of a h-Graphene dispersion (see details in Experimental Section). The film was then subjected to HT Joule heating by applying different bias voltages. Spectral radiance spectra of the heated film (Figure 3b) were acquired in order to

determine the actual film temperatures induced by the bias voltages. The spectra were then fitted to Planck's law assuming constant emissivity (solid black curves in Figure 3b), showing the achieved temperature range of $\sim 1300 - 2700$ K. Figure 3c depicts the morphology of h-Graphene film after 2700 K HT treatment. Surprisingly, no obvious nano-holes can be found and the graphene nanosheets seem to connect together into a continuous and smooth structure, this is in stark contrast to the as-prepared h-Graphene film as shown in Figure 2d. Higher magnification image (Figure S3) confirms the continuous graphene sheet without obvious nano-holes. TEM image shows that the HT treated h-Graphene nanosheets (Figure 3d) are similar to exfoliated graphene nanosheets from graphite^[21], confirming the absence of nano-holes on HT treated h-Graphene nanosheets. Higher magnification image displays the typical crystalline graphene lattice, indicating the high crystallization graphene structure from the 2700 K HT treatment (Figure 3e).

Similar healing characteristics were also found on larger scale h-Graphene macrostructures or assemblies obtained from solvent-free dry compression. The h-Graphene assembly with a predefined bar shape (length: 30mm, width: 6mm, thickness: 1mm) was obtained by pressing h-Graphene nanosheets in the designed mold under completely solvent-free conditions (Figure 3f). The fabricated h-Graphene assembly exhibited excellent mechanical stability, retaining the shape after both 2-m height dropping test and HT treatment (inset in Figure 3f). The starting graphene nanosheets are much less compressible due to the lack of an air escape mechanism during compression as well as the resistance of the nanosheets to stack together^[38]. As shown in Figure 3g, the assembly from the pristine graphene was only loosely bound after dry pressing and easily broke into pieces after a similar 2-m height dropping test (inset in Figure 3g). The cross-sectional SEM image of the 2700 K HT treated h-Graphene assembly showed that the graphene layers were

closely packed (Figure 3h), enabling good contacts among the laterally aligned graphene nanosheets across the entire vertical direction. HRTEM image confirms the high crystallization structure without nano-holes of 2700 K HT treated h-Graphene (Figure 3i). The tight packing and inter-contacting structure led to a highly dense graphene assembly and induced a continuous pathway for electrons and phonons to transport efficiently, resulting in greatly improved electrical conductivity and thermal conductivity.

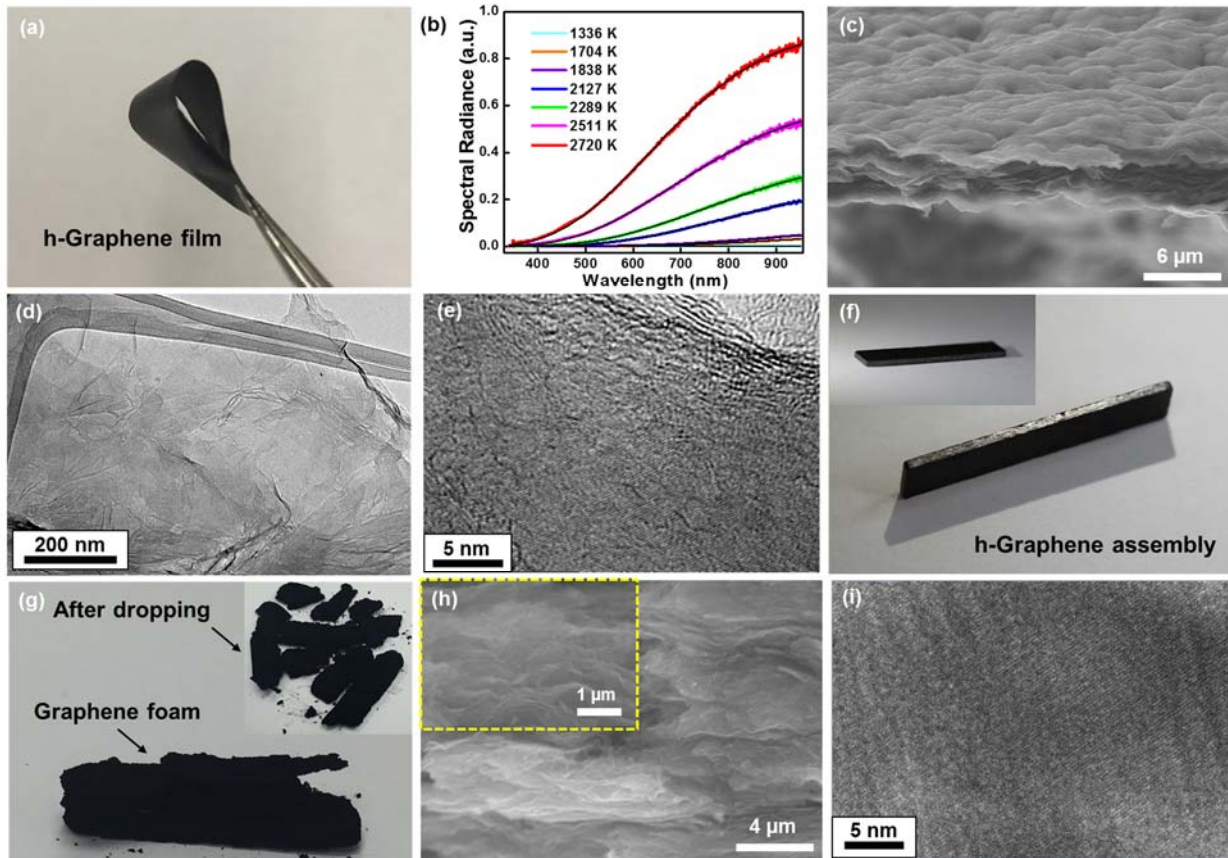


Figure 3 (a) Digital image of a flexible h-Graphene film fabricated by vacuum filtration. (b) Spectral radiance measurement of the same film sample at different bias voltages; temperature is determined by fitting the spectra to Planck’s law assuming constant emissivity. (c) SEM on the cross-sectional morphology of the 2700 K HT treated h-Graphene film. TEM images at (d) lower and (e) higher magnifications of the same 2700 K HT treated h-Graphene film sample. (f) Digital

image showing a dry-compressed h-Graphene bar assembly (length: 30mm, width: 6mm, thickness: 1mm). Inset shows that the assembly remained intact after a 2-m height dropping test. (g) Digital image of a dry-compressed assembly from the pristine graphene. Inset shows the damaged assembly after a similar 2-m height dropping test. (h) SEM images of the cross-sectional morphology of the 2700 K HT treated h-Graphene assembly. Inset shows the morphology at a higher magnification. (i) HRTEM image of the same 2700 K HT treated h-Graphene assembly.

Based on the experimental and modeling results, we propose a “hole-filling” mechanism that at the high temperature of 2700K, the nano-holes can be filled in by carbon radicals in the local environment such as small graphitic pieces or edge carbons of other graphene sheets. Molecular dynamics simulations were applied to investigate the hole-filling (carbon atoms reconstruction) behavior in a system where initially there is a monolayer graphene with a hole defect and a number of dispersed carbon radicals (Figure 4 (a) and (b)). The simulation was maintained at 2700 K (simulation details and extended data are shown in Figure S4~S5, supplementary information). The hole was observed to be filled by carbon radicals after 175 ps (Figure 4 (c) and (d)). The above modeling results agree with recent reports on defect healing^[48,49]. The filtered atomic-resolution TEM image of a 2700 K HT treated h-Graphene film also reveals the highly ordered arrangement of C6 rings, verifying the carbon atoms reconstruction derived from h-Graphene (Figure 4e).

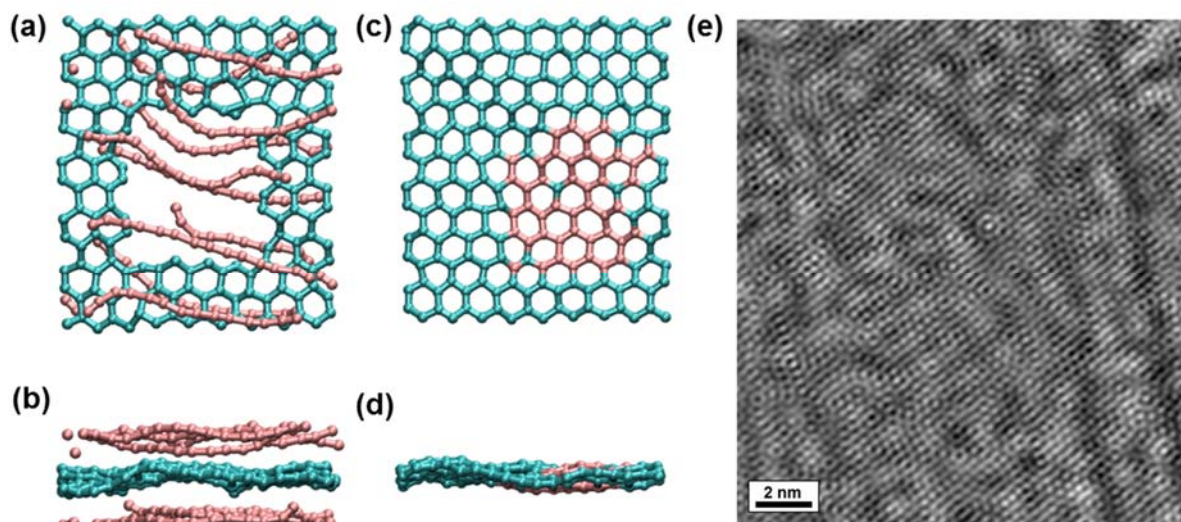


Figure 4 Molecular dynamics simulation results illustrating the carbon radicals filling in nano-holes in monolayer graphene at 2700 K. Cyan: carbon atoms that are initially from a monolayer graphene with a nano-hole defect at the center. Pink: carbon radicals. (a) Top view before the hole defect is filled. (b) Side view of (a). (c) Top view after the hole defect is filled. (d) Side view of (c). For visual clarity, the carbon radicals that have not filled the hole defect are not shown. (e) Filtered atomic-resolution TEM image of h-graphene after 2700 K high temperature treatment.

The intrinsic structure and chemical compositions of h-Graphene after HT treatment were investigated to understand the process of creating and repairing holes on graphene nanosheets. Figure 5a shows Raman spectra of three HT treated h-Graphene films under different temperatures (1000 K, 2000 K, 2700 K) for comparing the structure evolution upon heating. G band ($\sim 1,580 \text{ cm}^{-1}$) and 2D band ($\sim 2,700 \text{ cm}^{-1}$), both related to crystalline graphitic structures, were clearly visible under all conditions. However, the D bands ($\sim 1,350 \text{ cm}^{-1}$), an indicator of defects, were only apparent with strong intensity in the cases of h-Graphene films treated at 1000 K and 2000 K, with D-to-G ratio (I_D/I_G) of 1.2 and 0.75, respectively. For the case of 2700 K HT treated h-Graphene film, the D peak intensity was very low with an I_D/I_G ratio of 0.11, indicating the highly

crystalline structure. These Raman spectra suggests that the 2700 K HT treated h-Graphene closely approach defect-free graphene, and the very weak D peak may be caused by the edge effects and the negligible functional groups. X-ray diffraction (XRD) was employed to investigate the layered structure and d -spacing of 2700 K h-Graphene (HT treated, closed holes) and the as-prepared h-Graphene (open holes). 2700 K HT treated h-Graphene exhibited a sharp peak at $\sim 26.55^\circ$, while the as-prepared h-Graphene only showed a broad peak at $\sim 24.98^\circ$, consistent with the high graphitic crystallinity induced by HT Joule heating (Figure 5b). It is worth noting that the d -spacing ($d = 0.357$ nm) of the as-prepared h-Graphene decreases to 0.335 nm after 2700 K treatment, very near the value of graphite (~ 0.334 nm), which suggests the dense stacking of h-Graphene nanosheets with closed holes after high temperature treatment. X-ray photoelectron spectral (XPS) studies revealed that the C/O atomic ratio of h-Graphene significantly increased from 8.53 to 16.54 after 2700 K HT treatment (Figure 5c), indicating the effective removal of oxygen functional groups existing on h-Graphene. The full width at half maximum (FWHM) of the high resolution C 1s XPS spectra of 2700 K treated h-Graphene (0.75 eV) is narrower than that of the as-prepared sample (0.92 eV), further confirming the improved crystallinity after 2700 K HT treatment (Figure 5d).

The 2700 K HT treated h-Graphene film (thickness ~ 5 μm) with closed holes achieved an ultra-high room temperature electrical conductivity of 2209 S/cm. As shown in the I - V curves of a h-Graphene sample tested at room temperature (Figure 5e), the electrical conductivity of h-Graphene increases from ~ 128 S/cm to ~ 2209 S/cm after 2700 K HT treatment, an improvement of ~ 17 -fold. Hall measurement of the HT treated h-Graphene with closed holes confirmed the ultrahigh conductivity, and the excellent transport characteristics as indicated by the high carrier mobility of

673 $\text{cm}^2\text{V}^{-1}\text{s}^{-1}$ with a carrier density of $1.03 \times 10^{19} \text{ cm}^{-3}$. In comparison, as-prepared h-Graphene exhibited much lower carrier mobility ($26 \text{ cm}^2\text{V}^{-1}\text{s}^{-1}$) and carrier density ($3.3 \times 10^{19} \text{ cm}^{-3}$) (Figure 5f~5g). The aforementioned carrier mobility of h-Graphene with closed holes is among the highest carrier mobility for state of the art graphene films. Typical carrier mobility values for graphene films are usually between 0.1 and $365 \text{ cm}^2\text{V}^{-1}\text{s}^{-1}$ as reported in the literature (Figure 5h)^[50–53]. Note that although we didn't conduct the thermal conductivity property test, it is predictable that the HT treated h-Graphene film should possess an ultra-high thermal conductivity^[37,54].

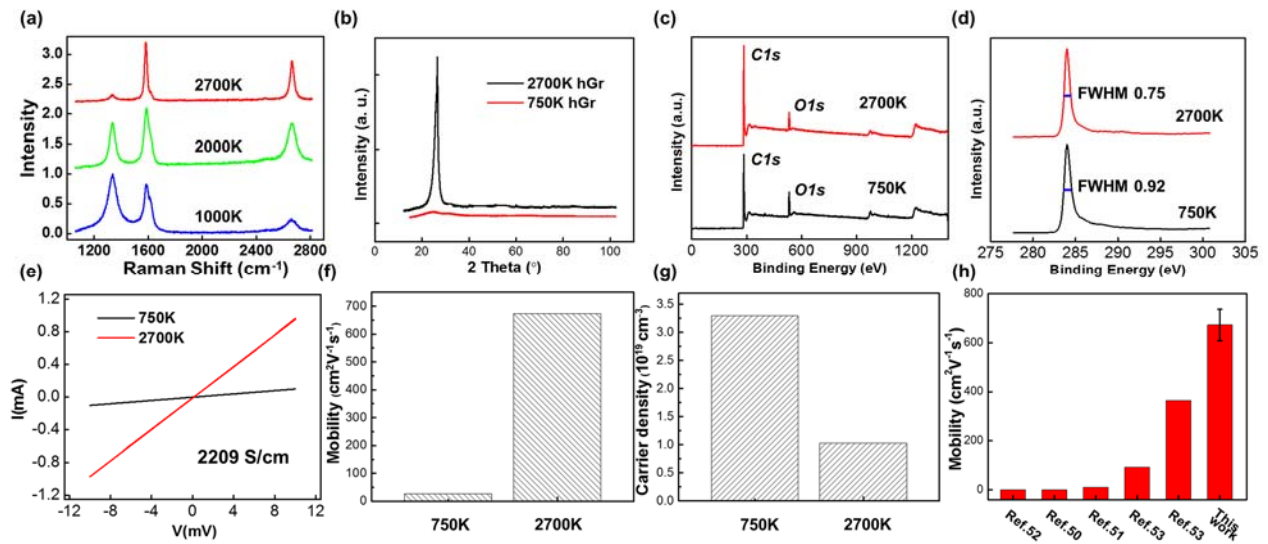


Figure 5 (a) Raman spectra of h-Graphene films that have been thermal treated at 1000 K, 2000 K and 2700 K respectively. (b) Representative XRD patterns, (c) XPS survey scans, and (d) C1s XPS spectra of a h-Graphene film before and after HT treatment at 2700 K. (e) *I-V* curves for a h-Graphene film before and after HT treatment at 2700 K. (f) The h-Graphene sample after 2700 K treatment exhibits a high carrier mobility of $673 \text{ cm}^2\text{V}^{-1}\text{s}^{-1}$ compared with the low carrier mobility of $26 \text{ cm}^2\text{V}^{-1}\text{s}^{-1}$ for an untreated film. (g) The h-Graphene film after 2700 K treatment has a carrier density of $1.03 \times 10^{19} \text{ cm}^{-3}$ compared with the carrier density of $3.3 \times 10^{19} \text{ cm}^{-3}$ for an untreated film. (h) Mobility of graphene samples reported in the literature.

Conclusion

In this study, we demonstrated that heating graphene nanosheets in hot air resulted in the creation of nano-holes, which can be subsequently repaired after being treated at HT of 2700 K. The h-Graphene can be fabricated into dense films by solution-based process (i.e., vacuum filtration) due to fast solvent escape through the holes on graphene nanosheets. The h-Graphene can even be directly compressed into a dense assembly under completely solvent-free conditions, opening up a new strategy for fast manufacturing of high-quality graphene based architectures. The highly dense graphene film or assembly with holes can be transformed to hole-free, highly crystalline graphene architecture after fast HT treatment via Joule heating. The HT treated h-Graphene exhibits excellent transport characteristics with ultrahigh electrical conductivity of 2209 S/cm, due to the high carrier mobility ($673 \text{ cm}^2\text{V}^{-1}\text{s}^{-1}$) of graphene nanosheets with closed holes. The proposed mechanism of repairing nano-holes on graphene nanosheets, supported by molecular dynamics (MD) modeling, is that carbon atoms recombine and carbon radicals fill in the holes under high temperature, creating a near-perfect carbon lattice consistent with that of graphene. We envision that the strategy of creating and repairing holes on graphene nanosheets utilizing thermal treatment provides new tools to tune defects on graphene and a new route to rapidly manufacture graphene materials with excellent performance in applications requiring high electrical and thermal conductivity.

Experimental Section

Synthesis of h-Graphene

1.5 g pristine graphene powder (Vorbeck Materials; Vor-X reduced 070) was placed in a quartz crucible and heated in air at a ramp rate of 10 K/min and held at 710 K for 10 h in an open-ended tube furnace (MTI Corporation). After cooling to room temperature, ~ 1.1-1.2 g h-Graphene was obtained as black powder.

Fabrication of h-Graphene film and assembly

The h-Graphene film was fabricated by vacuum filtration. Briefly, 0.2 g of as-synthesized h-Graphene powder was added to 200 mL of *N*-methyl-2-pyrrolidone (NMP) solution and the mixture was then sonicated for 3 h to disperse the h-Graphene nanosheets. A free-standing h-Graphene film with diameter of 35 mm was obtained by filtering the supernatant through a 0.65 μm pore-sized membrane (Millipore, U.S.A) with subsequent drying in air.

The h-Graphene article was fabricated by solvent-free compression molding at room temperature. 0.16 g of as-synthesized h-Graphene powder was transferred to a stainless steel die (length: 30 mm, width: 6 mm, thickness: 0.67 mm). In order to prevent the graphene assembly from sticking to the die, h-Graphene powder was sandwiched between two pieces of porous polypropylene (PP) membrane. H-Graphene assembly with a density of 1.05 g/cm^3 was finally obtained after cold-press using a hydraulic press (SPEX Sample Prep-Carver) with applied pressure (270 MPa) for 30 min.

Material characterization

A Hitachi SU-70 field emission scanning electron microscope (SEM), and a JEOL JEM 2100 transmission electron microscope (TEM) at an accelerating voltage of 200 kV were employed to characterize the morphology of graphene samples with open or closed holes. Micro-Raman

analysis was performed on a commercial Raman spectrometer (Labram Aramis model, Horiba Jobin Yvon) using a 633 nm He-Ne laser. XRD patterns were obtained using the D8 Advance (Bruker AXS, WI, USA). XPS data were acquired on a Kratos Axis 165 x-ray photoelectron spectrometer.

Temperature characterization

The high temperature treatment on sample was induced by direct Joule heating in an argon-filled glovebox. A custom-built spectrometer coupled optical fiber was used to capture the light induced by the high temperature of the sample, and then the recorded spectral radiance was fitted to Blackbody radiation to obtain the real-time temperature.

Conductivity and mobility measurement

Four-point probe measurements of longitudinal resistivity (ρ_{xx}) and Hall resistivity (ρ_{xy}) of the h-graphene samples were conducted by lock-in techniques at a low frequency of 3.7 Hz in a commercial cryostat (Quantum Design PPMS-9). The Hall voltage, in both magnetic field polarities, was measured and anti-symmetrized to exclude longitudinal voltage components.

Molecular dynamics simulations

The full atomistic simulations uses the ReaxFF potential as implemented in the LAMMPS (Large-scale Atomic/Molecular Massively Parallel Simulator) simulation package. The construction of model is shown in Figure S4a (supplementary information). Periodical boundary conditions are applied in the plane of graphene (x-y direction). The simulation box size is 2.21 nm by 2.56 nm by 0.81nm. Reflective wall boundary condition is applied at the boundary along z direction (out of plane of graphene) so that this boundary would reflect any atoms when they attempt to move through it. Such setting mimic the constant feeding of carbon radicals. The system is subjected to

NVT ensemble at a temperature of 2700K, using Nosé-Hoover thermostat. The time step is 0.25 fs.

Acknowledgement

L.H. and Y.C. acknowledge the support of NSF grants (1635221). We acknowledge the support of the Maryland NanoCenter and its NispLab. Y.L. and J.W.C acknowledge the financial support from the NASA Langley Internal Research and Development (IRAD) Program.

Appendix A. Supplementary data

Supplementary data associated with this article can be found, in the online version.

Reference

- [1] A. K. Geim, K. S. Novoselov, *Nat. Mater.* **2007**, *6*, 183.
- [2] A. A. Balandin, S. Ghosh, W. Bao, I. Calizo, D. Teweldebrhan, F. Miao, C. N. Lau, *Nano Lett.* **2008**, *8*, 902.
- [3] Y. Chen, G. C. Egan, J. Wan, S. Zhu, R. J. Jacob, W. Zhou, J. Dai, Y. Wang, V. A. Danner, Y. Yao, K. Fu, Y. Wang, W. Bao, T. Li, M. R. Zachariah, L. Hu, *Nat. Commun.* **2016**, *7*, 12332.
- [4] B. Wang, B. V. Cunnig, S.-Y. Park, M. Huang, J.-Y. Kim, R. S. Ruoff, *ACS Nano* **2016**, *10*, 9794.
- [5] Y. Yao, K. Fu, C. Yan, J. Dai, Y. Chen, Y. Wang, B. Zhang, E. M. Hitz, L. Hu, *ACS Nano* **2016**.
- [6] Y. Chen, Y. Li, Y. Wang, K. Fu, V. A. Danner, J. Dai, S. D. Lacey, Y. Yao, L. Hu, *Nano Lett.* **2016**, *16*, 5553.
- [7] C. Lee, X. Wei, J. W. Kysar, J. Hone, *Science* **2008**, *321*, 385.
- [8] X. Xie, G. Yu, N. Liu, Z. Bao, C. S. Criddle, Y. Cui, *Energy Environ. Sci.* **2012**, *5*, 6862.
- [9] D. Lin, Y. Liu, Z. Liang, H.-W. Lee, J. Sun, H. Wang, K. Yan, J. Xie, Y. Cui, *Nat. Nanotechnol.* **2016**, *11*, 626.
- [10] H. Wang, Y. Yang, Y. Liang, G. Zheng, Y. Li, Y. Cui, H. Dai, *Energy Environ. Sci.* **2012**, *5*, 7931.
- [11] N. Li, Z. Chen, W. Ren, F. Li, H.-M. Cheng, *Proc. Natl. Acad. Sci.* **2012**, *109*, 17360.
- [12] F. Bonaccorso, L. Colombo, G. Yu, M. Stoller, V. Tozzini, A. C. Ferrari, R. S. Ruoff, V. Pellegrini, *Science* **2015**, *347*, 1246501.
- [13] Y. Zhu, S. Murali, W. Cai, X. Li, J. W. Suk, J. R. Potts, R. S. Ruoff, *Adv. Mater.* **2010**, *22*, 3906.
- [14] H. Chen, F. Guo, Y. Liu, T. Huang, B. Zheng, N. Ananth, Z. Xu, W. Gao, C. Gao, *Adv. Mater.* **2017**, *29*, n/a.
- [15] N. Liu, H. Tian, G. Schwartz, J. B.-H. Tok, T.-L. Ren, Z. Bao, *Nano Lett.* **2014**, *14*, 3702.
- [16] Y. Li, H. Wang, L. Xie, Y. Liang, G. Hong, H. Dai, *J. Am. Chem. Soc.* **2011**, *133*, 7296.
- [17] Z. Chen, C. Xu, C. Ma, W. Ren, H.-M. Cheng, *Adv. Mater.* **2013**, *25*, 1296.
- [18] Y. Liu, H. Liang, Z. Xu, J. Xi, G. Chen, W. Gao, M. Xue, C. Gao, *ACS Nano* **2017**, *11*, 4301.
- [19] Y. Liu, Z. Xu, J. Zhan, P. Li, C. Gao, *Adv. Mater.* **2016**, *28*, 7941.
- [20] Y. Su, V. G. Kravets, S. L. Wong, J. Waters, A. K. Geim, R. R. Nair, *Nat. Commun.* **2014**, *5*, 5843.
- [21] X. Han, Y. Chen, H. Zhu, C. Preston, J. Wan, Z. Fang, L. Hu, *Nanotechnology* **2013**, *24*, 205304.
- [22] Y. L. Zhong, Z. Tian, G. P. Simon, D. Li, *Mater. Today* **2015**, *18*, 73.
- [23] H. Chen, M. B. Müller, K. J. Gilmore, G. G. Wallace, D. Li, *Adv. Mater.* **2008**, *20*, 3557.
- [24] D. R. Dreyer, S. Park, C. W. Bielawski, R. S. Ruoff, *Chem. Soc. Rev.* **2009**, *39*, 228.
- [25] D. Li, M. B. Müller, S. Gilje, R. B. Kaner, G. G. Wallace, *Nat. Nanotechnol.* **2008**, *3*, 101.
- [26] D. Li, R. B. Kaner, *Science* **2008**, *320*, 1170.
- [27] Z. Li, Z. Xu, Y. Liu, R. Wang, C. Gao, *Nat. Commun.* **2016**, *7*, 13684.
- [28] Z. Xu, Y. Liu, X. Zhao, L. Peng, H. Sun, Y. Xu, X. Ren, C. Jin, P. Xu, M. Wang, C. Gao, *Adv. Mater.* **2016**, *28*, 6449.

- [29] Z.-S. Wu, W. Ren, L. Gao, J. Zhao, Z. Chen, B. Liu, D. Tang, B. Yu, C. Jiang, H.-M. Cheng, *ACS Nano* **2009**, *3*, 411.
- [30] Z. Xu, Y. Zhang, P. Li, C. Gao, *ACS Nano* **2012**, *6*, 7103.
- [31] S. Park, R. S. Ruoff, *Nat. Nanotechnol.* **2010**, *5*, 309.
- [32] I. K. Moon, J. Lee, R. S. Ruoff, H. Lee, *Nat. Commun.* **2010**, *1*, 73.
- [33] A. Bagri, C. Mattevi, M. Acik, Y. J. Chabal, M. Chhowalla, V. B. Shenoy, *Nat. Chem.* **2010**, *2*, 581.
- [34] L. J. Cote, R. Cruz-Silva, J. Huang, *J. Am. Chem. Soc.* **2009**, *131*, 11027.
- [35] S. Pei, J. Zhao, J. Du, W. Ren, H.-M. Cheng, *Carbon* **2010**, *48*, 4466.
- [36] S. Pei, H.-M. Cheng, *Carbon* **2012**, *50*, 3210.
- [37] G. Xin, T. Yao, H. Sun, S. M. Scott, D. Shao, G. Wang, J. Lian, *Science* **2015**, *349*, 1083.
- [38] X. Han, M. R. Funk, F. Shen, Y.-C. Chen, Y. Li, C. J. Campbell, J. Dai, X. Yang, J.-W. Kim, Y. Liao, J. W. Connell, V. Barone, Z. Chen, Y. Lin, L. Hu, *ACS Nano* **2014**, *8*, 8255.
- [39] L. Jiang, Z. Fan, *Nanoscale* **2014**, *6*, 1922.
- [40] H. Li, Y. Tan, P. Liu, C. Guo, M. Luo, J. Han, T. Lin, F. Huang, M. Chen, *Adv. Mater.* **2016**, *28*, 8945.
- [41] Y. Ito, Y. Shen, D. Hojo, Y. Itagaki, T. Fujita, L. Chen, T. Aida, Z. Tang, T. Adschiri, M. Chen, *Adv. Mater.* **2016**, *28*, 10644.
- [42] Y. Lin, X. Han, C. J. Campbell, J.-W. Kim, B. Zhao, W. Luo, J. Dai, L. Hu, J. W. Connell, *Adv. Funct. Mater.* **2015**, *25*, 2920.
- [43] Y. Lin, K. A. Watson, J.-W. Kim, D. W. Baggett, D. C. Working, J. W. Connell, *Nanoscale* **2013**, *5*, 7814.
- [44] H. Sun, L. Mei, J. Liang, Z. Zhao, C. Lee, H. Fei, M. Ding, J. Lau, M. Li, C. Wang, X. Xu, G. Hao, B. Papandrea, I. Shakir, B. Dunn, Y. Huang, X. Duan, *Science* **2017**, *356*, 599.
- [45] Y. Xu, Z. Lin, X. Zhong, X. Huang, N. O. Weiss, Y. Huang, X. Duan, *Nat. Commun.* **2014**, *5*, ncomms5554.
- [46] S. P. Surwade, S. N. Smirnov, I. V. Vlassioug, R. R. Unocic, G. M. Veith, S. Dai, S. M. Mahurin, *Nat. Nanotechnol.* **2015**, *10*, 459.
- [47] S. J. Heerema, C. Dekker, *Nat. Nanotechnol.* **2016**, *11*, 127.
- [48] A. Barreiro, F. Börrnert, S. M. Avdoshenko, B. Rellinghaus, G. Cuniberti, M. H. Rummeli, L. M. K. Vandersypen, *Sci. Rep.* **2013**, *3*.
- [49] A. Barreiro, F. Börrnert, M. H. Rummeli, B. Büchner, L. M. K. Vandersypen, *Nano Lett.* **2012**, *12*, 1873.
- [50] G. Eda, G. Fanchini, M. Chhowalla, *Nat. Nanotechnol.* **2008**, *3*, 270.
- [51] S. Wang, P.-J. Chia, L.-L. Chua, L.-H. Zhao, R.-Q. Png, S. Sivaramakrishnan, M. Zhou, R. G.-S. Goh, R. H. Friend, A. T.-S. Wee, P. K.-H. Ho, *Adv. Mater.* **2008**, *20*, 3440.
- [52] G. Eda, M. Chhowalla, *Nano Lett.* **2009**, *9*, 814.
- [53] S. Wang, P. K. Ang, Z. Wang, A. L. L. Tang, J. T. L. Thong, K. P. Loh, *Nano Lett.* **2010**, *10*, 92.
- [54] C. Teng, D. Xie, J. Wang, Z. Yang, G. Ren, Y. Zhu, *Adv. Funct. Mater.* **2017**, *27*, 1700240.

Supplementary Information

Nanomanufacturing of Graphene Nanosheets through Hole Engineering

Yanan Chen^{1, (a)}, Yilin Wang^{1, (a)}, Shuze Zhu², Kun Fu¹, Xiaogang Han¹, Yanbin Wang¹, Bin Zhao¹, Tian Li¹, Boyang Liu¹, Yiju Li¹, Jiaqi Dai¹, Teng Li², John W. Connell³, Yi Lin^{4, *}, Liangbing Hu^{1, *}

¹Department of Materials Science and Engineering, University of Maryland College Park, College Park, Maryland, 20742

²Department of Mechanical Engineering, University of Maryland College Park, College Park, Maryland, 20742

³Advanced Materials and Processing Branch, NASA Langley Research Center, Hampton, VA 23681-2199

⁴National Institute of Aerospace, 100 Exploration Way, Hampton, Virginia 23666-6147

(a) Contributed equally to this work.

Email: binghu@umd.edu; yi.lin-1@nasa.gov

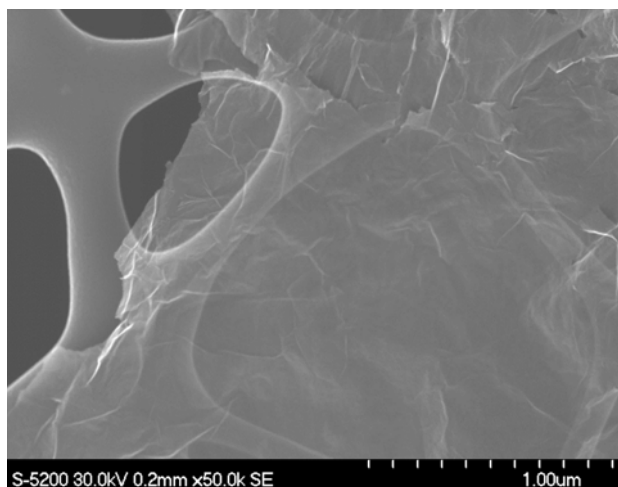


Figure S1 SEM image of a pristine graphene nanosheet.

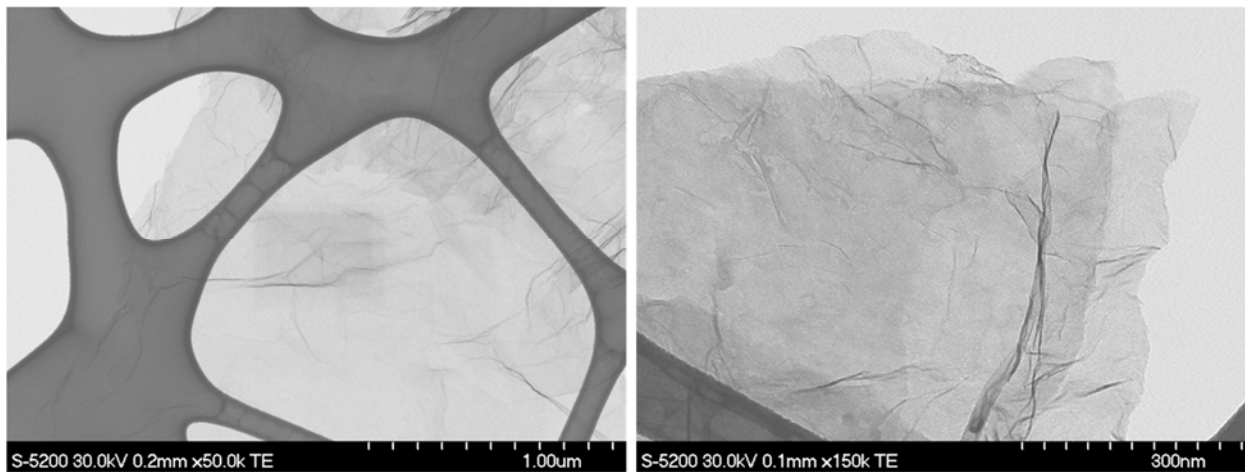


Figure S2 TEM images of pristine graphene nanosheets.

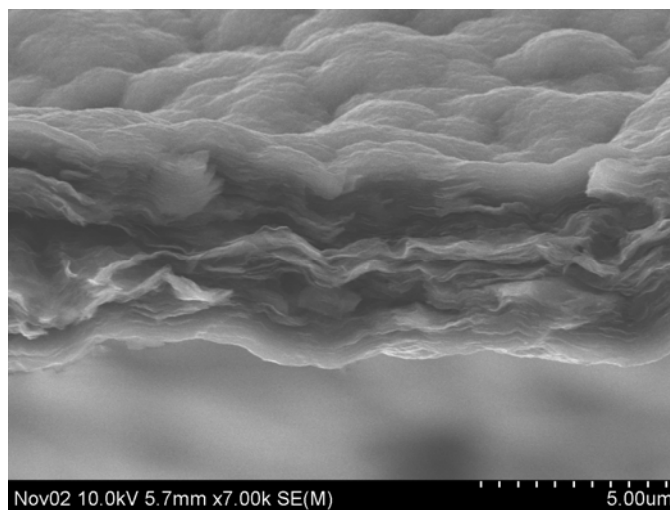


Figure S3 High magnification SEM image showing details of surface morphology of a 2700 K HT treated h-Graphene film.

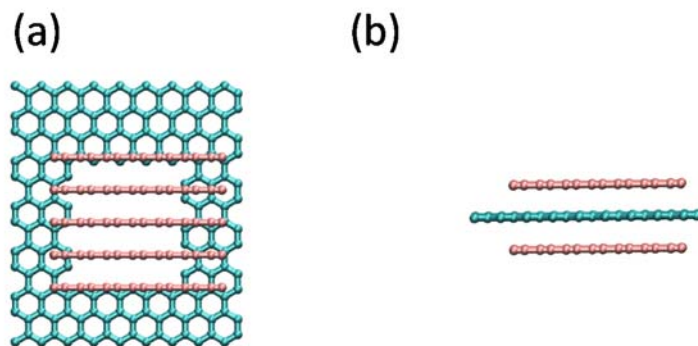


Figure S4 (a) Initial model. Periodical boundary conditions are applied in the plane of graphene. Cyan: a monolayer graphene with a hole defect at the center. Pink: carbon radicals. (b) side view of (a).

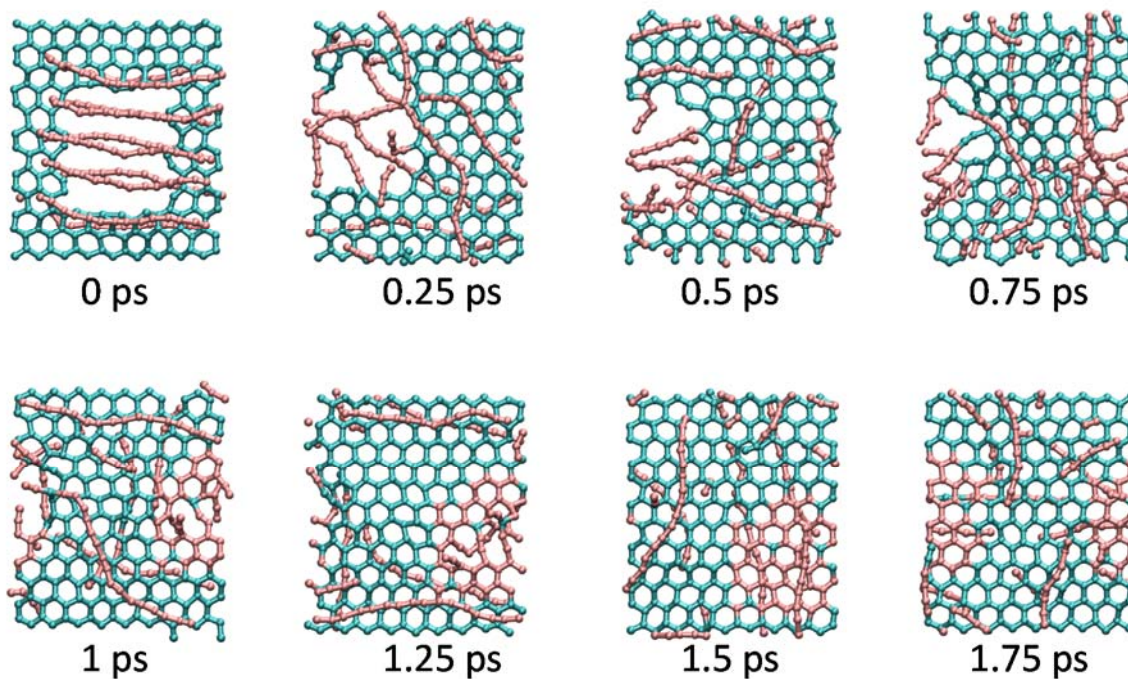


Figure S5 Sequential snapshots of the hole-filling process. Pink: carbon radicals. The edge of the hole reconstructs at high temperature with the introduction of additional carbon radicals. With a constant feeding of carbon radicals at a high temperature of 2700 K, bonds are formed gradually between the edge atoms and carbon radicals until the hole is filled.